THE ASTROPHYSICAL JOURNAL, 567:1272–1275, 2002 March 10

CHARGE TRANSFER OF O^{5+} AND O^{4+} WITH CO AT keV ENERGIES

H. GAO AND VICTOR H. S. KWONG
Physics Department, University of Nevada at Las Vegas, 4505 South Maryland Parkway, Las Vegas, NV 89154-4002
Received 2001 September 15; accepted 2001 November 9

ABSTRACT

Charge transfer emission has been reported to be the dominant source of X-rays in cometary atmospheres. The emission model is based on the estimated charge transfer cross sections of solar wind minor/heavy ions and cometary neutrals. We report the results of our measurements on the absolute total one and multielectron transfer cross sections for O^{q+} ($q = 5$, 4) with CO at $\sim 1.5q$ keV energies using a technique that combines a laser ablation ion source and a reflection time-of-flight mass spectrometer. The total single electron transfer cross sections for O^{5+} and O^{4+} ions with CO are $3.42(\pm 0.50) \times 10^{-15}$ and $2.91(\pm 0.41) \times 10^{-15}$ cm^2, respectively. The cross sections for multielectron transfer are $1.15(\pm 0.37) \times 10^{-15}$ and $1.03(\pm 0.28) \times 10^{-15}$ cm^2, respectively.

Subject headings: atomic data — atomic processes — radiation mechanisms: nonthermal — solar wind — ultraviolet: general — X-rays: general

1. INTRODUCTION

Observations by the *ROSAT* satellite and the *Rossi X-Ray Timing Explorer* (*RXTE*) of extreme-ultraviolet (EUV) and X-ray emissions from the comet C/Hyakutake 1996 B2 have generated intense interest in the mechanisms of the X-ray source (Lisse et al. 1996). Review of the *ROSAT* X-ray all-sky survey conducted in 1990–1991 also shows X-ray emission from the comets C/Tsuchiya-Kiuchi 1990 XVII, C/Levy 1900 XX, C/Arai 1990 XXVI, and 45P/Honda-Mrkos-Padjusakova 1990, and from three of the brightest comets observed in the all-sky survey (Dennerl et al. 1996a, 1996b; Dennerl, Englhauser, & Trümper 1997).

Several X-ray emission mechanisms have been proposed. These mechanisms include scattering of solar X-rays, inner-shell ionization by solar wind ions and electrons, bremsstrahlung of solar wind electrons, collision between cometary and interplanetary dust particles, scattering, and bremsstrahlung by attogram dust particles, and charge transfer of the solar wind heavy ions with cometary molecules (Lisse et al. 1996, 2001; Wickramasinghe & Hoyle 1996; Northrop et al. 1997; Bingham et al. 1997; Cravens 1997; Krasnopolsky et al. 1997; Krasnopolsky 1998; Krasnopolsky & Mumma 2001; Haberli et al. 1997; Mumma, Krasnopolsky, & Abbott 1997; Wegmann et al. 1998). Of all these mechanisms, only the last two have shown promise in quantitatively explaining the X-ray emission spectra of cometary atmospheres (Owens et al. 1998).

Solar wind contains a large number of minor/heavy ion species with a range of charge states, such as O^{6+}, C^{5+}, N^{5+}, and Si^{10+} (Cravens 1997). These ions will readily charge transfer with cometary neutrals such as H_2O, CO, CO_2, OH, and O-producing product ions that can be highly excited and subsequently emit photons in the EUV and X-ray. A qualitative modeling of cometary X-rays generated by solar wind minor/heavy ions was carried out by Cravens (1997), Haberli et al. (1997), Krasnopolsky (1997), Mumma et al. (1997), Wegmann et al. (1998), and Kharchenko & Dalgarno (2000). These investigators have concluded that charge transfer between solar wind minor/heavy ions and cometary neutrals is the dominant mechanism for X-ray emission in comets. However, in their modeling of X-ray emission from cometary atmospheres, either calculated charge transfer cross sections based on Landau-Zener approximation or cross sections extrapolated from the experimental values between O^{6+}, C^{5+} ions and H and H_2 (Phaneuf et al. 1982; Janev & Winter 1985; Janev, Phaneuf, & Hunter 1988; Dijkkamp et al. 1985; Suraud et al. 1991) were used. No quantal calculation or direct experimental cross sections were available at this energy range for the charge transfer between solar wind ions and major cometary neutrals. These estimates ($\sim 10^{-15}$ cm^2) allow one to guess the order of magnitude of the total cross sections at best. Only recently have a few experimental cross sections and absolute theoretical cross sections begun to emerge (Greenwood et al. 2000; Hasan et al. 2001). The bandwidth of the *ROSAT* does not have enough resolution to identify all the emission lines. However, the high resolution capability of the *Chandra X-Ray Observatory* enables us to resolve individual spectral lines, thus giving us a better insight into the emission-line spectrum and therefore the source of the emission line. Both the charge transfer emission spectrum and the charge transfer cross sections are essential in the correct interpretation of the emission lines.

In this paper, we have extended our measurements to include the single and multielectron charge transfer cross sections of O^{q+} ($q = 5$, 4) with CO. In our recent charge transfer measurements (Gao, Fang, & Kwang 2001) of O^{q+} ($q = 3$, 2) with CO, we found that their respective single capture cross sections are 1.3 and 6.3 times larger than that of similar reaction with H_2. Furthermore, the double capture cross section for O^{3+} is about 57% of its single capture cross section. The major solar wind oxygen ions are highly stripped, i.e., O^{6+}. Nevertheless, charge transfer does not terminate at O^{5+}. The current single and multielectron capture measurements will provide information on the cascade contributions of the UV, EUV, and soft X-ray emission structure in cometary atmospheres. Experimental data can help to confirm and further refine the emission model.

2. MEASUREMENTS

Figure 1 shows a simplified schematic of a reflection time-of-flight mass spectrometer (RTOFMS) with a laser ablation ion source used in the current measurements of charge transfer cross sections of O^{5+} and O^{4+} with CO. A detailed

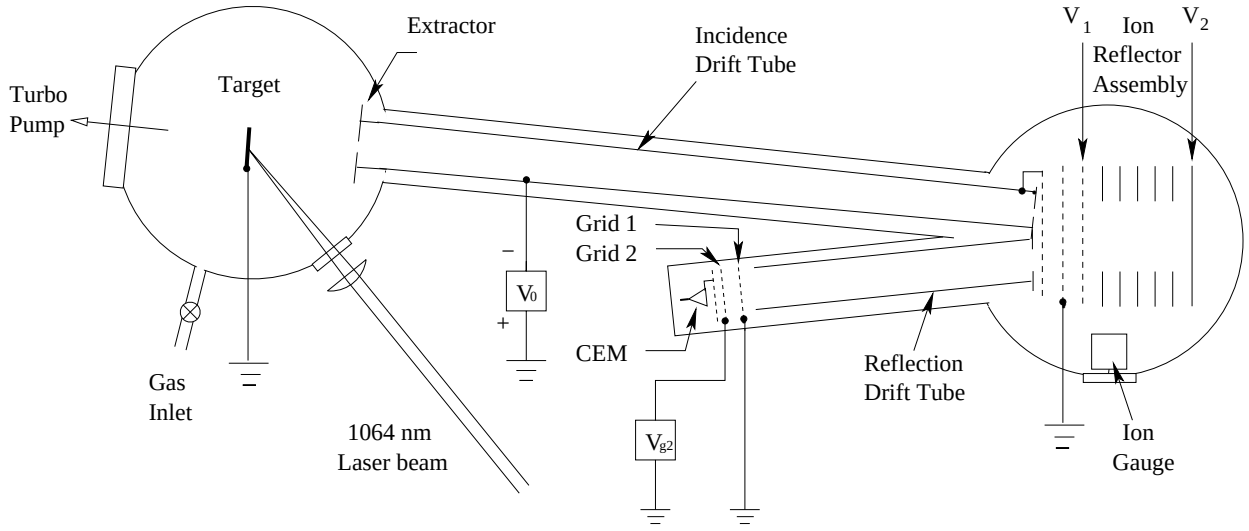

FIG. 1.—Simplified schematic of the reflection time-of-flight mass spectrometer (RTOFMS) used in the current measurement

description of this facility can be found in previous publications (Wang & Kwong 1997; Gao et al. 2001). Oxygen ions were produced by laser ablation of a high-purity (97%) solid Ta_2O_5 target mounted on a rotatable manipulator inside a vacuum reaction chamber. The energy of a 50 ns neodymium-doped yttrium aluminum garnet (Nd:YAG) laser pulse was about 180 mJ. At this power density, O^{q+} with q less than or equal to 5 were routinely produced. Ions of the laser ablation plasmas were extracted into the incident drift tube through a small aperture of an ion extraction plate at the entrance to the RTOFMS. Both the ion extraction plate and the incident drift tube were biased at $V_0 = -1500$ V relative to the ground. Ions of charge q produced by laser ablation acquired additional kinetic energy, $\delta E = -qeV_0$, from the extraction field and traveled at a constant drift velocity in the field-free incident drift tube. They were separated in their time-of-flight according to their mass-to-charge ratio. Since ions produced by laser ablation have a range of initial kinetic energies, E_i, the total kinetic energy of the ions with different charge states can overlap. This overlapping of the ion arrival time at the detector limits the mass resolution of the time-of-flight (TOF) spectrum. The spread of the TOF of these ions is reduced by reflecting the ions 168° into a reflection drift tube at the end of the incident drift tube by a reflector assembly. The reflector assembly consists of a highly transparent front plate and a solid backplate with several evenly spaced, highly transparent, potential gradient ring electrodes to maintain a uniform electric field. With this setup, ions with higher initial kinetic energy penetrate farther into the reflector assembly than the ions with lower initial kinetic energies before they are reflected into the reflection drift tube. The extra path taken by the more energetic ions allows the slower ions of the same q to catch up in time. By applying the appropriate potentials on the electrodes of the incident drift tube, the reflector assembly, and the reflection drift tube, ions of the same m/q but with different initial kinetic energies can arrive at the detector plane at about the same time. While the RTOFMS was used to focus the parent ions of different charge states at the detector plane, the charge transfer measurement was carried out inside the reflection drift tube. The following paragraph expands on this point.

With reference to Figure 1, the potentials of the front plate and the back plate of the reflector assembly were set at $V_1 = +70$ V and $V_2 = +800$ V, respectively. The potentials applied to those two electrodes were chosen for optimal beam intensity and mass resolution. Furthermore, product ions of O^{5+} and O^{4+} formed by charge transfer with CO during their transit inside the incident drift tube did not enter the reflection drift tube. The total kinetic energy of the product ion was $E_i + 1500$ eV for single electron capture (SC) and $E_i + 3000$ eV for double electron capture. Their trajectories after reflection from the reflector assembly were quite different from that of their parent ions with kinetic energies E_i. The trajectories of the product ions were beyond the acceptance angle of the reflection drift tube; thus, all product ions were blocked from entering the reflection drift tube. Only the parent oxygen ions within a narrow energy range and their product ions produced during transit inside the reflection drift tube as the result of charge transfer were detected by a channel electron multiplier (CEM) detector located at the end of the reflection drift tube.

Figure 2*a* is a typical TOF mass spectrum of O^{q+} ions. However, this TOF mass spectrum cannot be used to identify the product ions such as $O^{(q-n)+}$ ($n = 1, 2, 3$) through single electron capture ($n = 1$) and multielectron capture (MC; $n \geq 2$) from their parent ion O^{q+}, since the energy transfer between O^{q+} and CO is negligibly small in the charge transfer collision. Product ions have kinetic energy very similar to their parent ions after the reaction inside the reflection drift tube. To isolate the product ions from the parent ions, a potential barrier generated by a retardation electric field was applied to the ions at grid 2 between the end of the reflection drift tube and the CEM detector (see Fig. 1). The ions were first retarded by the grounded grid 1. Because of their charge differences, the kinetic energies of the parent ions and the product ions, after passing through grid 1, were reduced to E_i, $E_i - eV_0$, and $E_i - 2eV_0$ for O^{q+}, $O^{(q-1)+}$, and $O^{(q-2)+}$, respectively. By applying an appropriate potential V_{g2} at grid 2, parent and/or product oxygen ions of specific charge state with kinetic energy greater than the potential barrier will proceed toward the CEM and can be detected. For example, for $qeV_{g2} > E_i$ and $(q-1)eV_{g2} <$

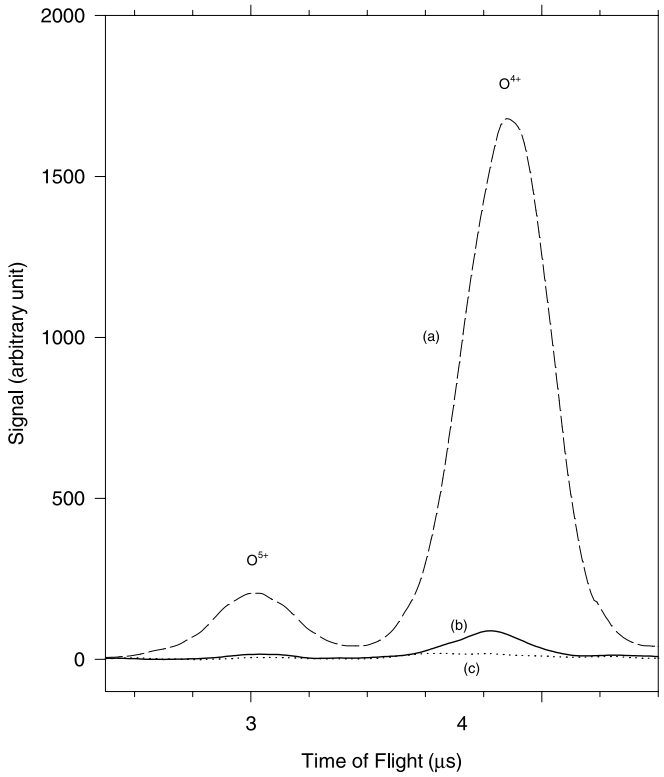

FIG. 2.—Typical time-of-flight mass spectra in the measurement of electron capture of O^{5+} and O^{4+} with CO. (*a*) Parent O^{5+} + product ions (*first peak*) and parent O^{4+} + product ions (*second peak*). (*b*) All single and multielectron capture product ions. Both parent ions are excluded. (*c*) All multielectron capture product ions. Parent and single electron capture product ions are excluded.

$E_i - eV_0$, parent ions O^{q+} will be blocked, while product ions $O^{(q-1)+}$ and $O^{(q-2)+}$ will pass through grid 2 and be detected by the CEM (Fig. 2*b*).

The range of kinetic energies, E_i, of the parent ions reflected into the reflection drift tube is obtained by analyzing the trajectories of the reflected ions within the acceptance angle of the reflection drift tube. The range of E_i for O^{5+} ion is 540–1650 eV, while the range for O^{4+} ion is 430–1330 eV. Based on the value of E_i and the acceleration potential of the drift tube V_0, V_{g2} was set to (1) 0 V to let the parent ions and their product ions reach the CEM, (2) +500 V to block both the parent O^{5+} and O^{4+} ions only, and (3) +1100 V to block the parent ions and the single capture product ions. Table 1 summarizes the relationship between the potentials applied at grid 2 and the parent and product ions that pass through the barrier and are detected by CEM.

The systematic uncertainties on the ion signal due to the laser energy fluctuation and the changes in the target surface conditions were reduced by repeating the measurements in preprogrammed cycles. In each cycle the potential, V_{g2}, applied at grid 2 was sequentially switched according to the values stated in the above discussion, i.e., 0, +500, and +1100 V. About 3000 measurements were made. The signals were recorded by a Tektronix digital oscilloscope. These signals were binned according to the switching sequence and stored in a computer for later analysis. Figure 2*a* shows two separate ion peaks (*dashed line*) located at about 3 and 3.9 μs. The first peak corresponds to the parent O^{5+} and its product ions, while the second peak corresponds to parent O^{4+} and its product ions. The intensity of each peak changes when a predetermined potential, V_{g2}, is applied at grid 2. Figure 2*b* shows the much weaker peaks (*solid line*) that correspond to all product ions formed by one or more electron transfer processes. Figure 2*c* shows the smallest peaks (*dotted line*) that correspond to the product ions formed by two or more electron transfer processes. These signal intensities are used to determine the charge transfer cross sections. The pressure of CO was measured by a calibrated ion gauge mounted at the entrance to the reflection drift tube. The calibration method has been discussed in a previous publication (Kwong et al. 1990). The CO pressure used in the experiment was 2.0×10^{-5} torr. The residual gas pressure of the reaction chamber was analyzed and monitored by a residual gas analyzer and was found to consist of mainly H_2, H_2O, and CO with a total pressure of less than 2×10^{-9} torr.

3. DATA ANALYSIS AND RESULTS

The electron capture cross section, σ, can be derived from the following expression:

$$\frac{I_p}{I_0} = 1 - e^{-\sigma nL}, \tag{1}$$

$$\sigma \approx \frac{I_p}{I_0 nL}, \tag{2}$$

TABLE 1

SCREENING OF PRODUCT IONS FROM THEIR PARENT IONS

V_{g2} (V)	PARENT ION	PRODUCT ION		
	O^{4+}, KE (eV) = (430, 1330)	O^{3+}, (1930, 2830)	O^{2+}, (3430, 4330)	O^+ and O^0 ≥ 4930
0.....	Pass	Pass	Pass	Pass
500.....	Blocked	Pass	Pass	Pass
1100.....	Blocked	Blocked	Pass	Pass
	O^{5+}, KE (eV) = (540, 1650)	O^{4+}, (2040, 3150)	O^{3+}, (3540, 4650)	O^{2+}, O^+ ≥ 5040 and O^0
0.....	Pass	Pass	Pass	Pass
500.....	Blocked	Pass	Pass	Pass
1100.....	Blocked	Blocked	Pass	Pass

NOTE.—Ions with kinetic energy greater than the potential barrier qeV_{g2} can pass through grid 2 and be detected by CEM. V_{g2} is the voltage applied at grid 2. The range of kinetic energies (KE) of the ions is determined by the acceptance angle of the reflection drift tube and the potentials applied to the reflector assembly.

TABLE 2

MEASURED CHARGE TRANSFER CROSS SECTION σ FOR O^{q+} ($q = 5, 4, 3, 2$) WITH CO

Reaction	Energy (eV)	σ(SC)[a] (10^{-15} cm^2)	σ(MC)[b] (10^{-15} cm^2)
O^{5+} + CO	8464 ± 690	3.42 ± 0.50	1.15 ± 0.37 (MC)[b]
O^{4+} + CO	6780 ± 555	2.91 ± 0.41	1.03 ± 0.28 (MC)
O^{3+} + CO[c].....	4860 ± 240	1.26 ± 0.18	0.72 ± 0.11 (DC)[c]
O^{2+} + CO[c].....	3240 ± 160	0.76 ± 0.11	

[a] SC: single electron capture.
[b] MC: multielectron capture.
[c] DC: double electron capture only (Gao et al. 2001).

where I_p is the signal intensity of the product oxygen ions, I_0 is the intensity of the parent O^{q+} ions, L is the physical interaction length of the reflection drift tube, and n is the density of the target CO gas. In equation (2), the approximation is valid because $I_p/I_0 \ll 1$ in our measurement, which also ensures the single collision condition. The ion energies are estimated to be 8464 ± 690 and 6780 ± 555 eV for O^{5+} and O^{4+}, respectively. The measured charge transfer cross sections are tabulated in Table 2, together with our previous measurement of O^{3+} and O^{2+} with CO.

The atomic structure of O^{5+} and O^{4+} is very complex. These ions can be produced in a wide range of energy states. The presence of metastable state ions in the parent ion beam may affect the measured electron capture cross sections. The radiative lifetime of the metastable state of O^{5+} ($1s2s2p\,^4P$) have been measured to be 1.0, 4.2, and 27 ns for $J = 1/2$, 3/2, and 5/2, respectively (Charalambidis, Brenn, & Koulen 1989). These ions will decay to their ground states before reaching the reflection drift tube where charge transfer measurement is made. They have no effect on our measurement. The metastable state lifetime of O^{4+} ($1s^22s2p\,^3P_1$), however, is much longer. Its radiative lifetime has been measured to be 0.5 ms (Doerfert et al. 1995). If these ions are in the beam and their short transit time (a few μs) in the incident drift tube does not allow them to relax to their ground states prior to the measurement, then the measured cross sections can be difficult to interpret.

The metastable fractions in the pulsed laser plasma ion source have been investigated experimentally by Kwong & Fang (1993) and Fang & Kwong (1994, 1995) in their charge transfer study of O^{2+} ($2s^22p^2\,^1D$ metastable state, $\tau \sim 37$ s, $2s^22p^2\,^1S$ metastable state, $\tau \sim 0.55$ s; Church & Holzscheiter 1989) using an RF trap, and Wang & Kwong (1997) in their electron capture study of C^{2+} ($2s2p\,^3P_{0,1,2}$ metastable states, $\tau \geq 8.26$ ms; Kwong & Fang 1993) using the same facility for the current measurement. In both cases, their results are in agreement with the ground-state measurements (Church & Holzscheiter 1989; Unterreiter, Schweinzer, & Winter 1991). This would suggest that the metastable fractions in the pulsed laser plasma ion source were negligibly small. We conclude that there is no significant contribution by the metastable state ions in the present measurements.

The gain efficiency of the detector depends on the ion charge state and its incident kinetic energy (Phaneuf et al. 1982). Since the CEM was operated in the analog mode, the gain efficiencies for O^{q+} ($q = 5, 4, 3, 2$) have to be experimentally determined. The calibration of the gain efficiency is carried out by measuring the pulse-height distribution of an individual oxygen ion of a specific charge state and kinetic energy. This was done by defocusing the ion beam with an electrostatic lens inside the incident drift tube until the individual ion was detected. No significant difference in the efficiency has been observed.

The uncertainty of the gas pressure is estimated to be about 8% from the absolute ion gauge calibration. The uncertainties introduced by the nonlinearity of the channel electron multiplier/preamplifier and the pulse-height calibration are about 2% and 11%, respectively. The uncertainty of the signal intensity is about the same for both O^{5+} and O^{4+}, less than 5% for single electron capture and up to 27% for multielectron transfer processes. The total absolute uncertainty for the cross section is about 14% for single electron capture and 30% for multielectron capture after a quadratic sum.

The authors thank Z. Fang, Bill O'Donnell, and Jennifer Pursley for their valuable technical assistance. This work is supported by the Nevada state EPSCoR program and by NASA under grant NAG5-6727 to UNLV.

REFERENCES

Bingham, R., Dawson, J. M., Shapiro, V. D., Mendis, D. A., & Kellet, B. J. 1997, Science, 275, 49
Charalambidis, D., Brenn, R., & Koulen, K. J. 1989, Phys. Rev. A, 40, 2359
Church, D. A., & Holzscheiter, H. M. 1989, Phys. Rev. A, 40, 54
Cravens, T. E. 1997, Geophys. Res. Lett., 24, 105
Dennerl, K., Englhauser, J., & Trümper, J. 1997, Science, 277, 1625
Dennerl, K., et al. 1996a, IAU Circ., 6404, 2
———. 1996b, IAU Circ., 6413, 2
Dijkkamp, D., Gordeev, Yu. S., Brazuk, A., Drentje, A. G., & de Heer., F. J. 1985, J. Phys. B, 18, 737
Doerfert, J., et al. 1995, Nucl. Instrum. Methods Phys. Res. B, 98, 53
Fang, Z., & Kwong, V. H. S. 1994, Rev. Sci. Instrum., 65, 2143
———. 1995, Phys. Rev. A, 51, 1321
Gao, H., Fang, Z., & Kwong, V. H. S. 2001, Phys. Rev. A, 63, c2704
Greenwood, J. B., Williams, I. D., Smith, S. J., & Chutjian, A. 2000, ApJ, 533, L175
Haberli, R. M., Gombosi, T. I., De Zeeuw, D. L., Combi, M. R., & Powell, K. G. 1997, Science, 276, 939
Hasan, A. A., Eissa, F., Ali, R., Schultz, D. R., & Stancil, P. C. 2001, ApJ, 560, L201
Janev, R. K., Phaneuf, R. A., & Hunter, H. T. 1988, At. Data Nucl. Data Tables, 40, 249
Janev, R. K., & Winter, H. 1985, Phys. Rep., 117, 265
Kharchenko, V., & Dalgarno, A. 2000, J. Geophys. Res., 105, 18351
Krasnopolsky, V. A. 1997, Icarus, 128, 368
———. 1998, J. Geophys. Res., 103, 2069
Krasnopolsky, V. A., & Mumma, M. J. 2001, ApJ, 549, 629
Krasnopolsky, V. A., Mumma, M. J., Abbott, M., Flynn, B. C., Meech, K. J., Yeomans, D. K., Feldman, P. D., & Cosmovici, C. B. 1997, Science, 277, 1488
Kwong, V. H. S., & Fang, Z. 1993, Phys. Rev. Lett., 71, 4127
Kwong, V. H. S., et al. 1990, Rev. Sci. Instrum., 61, 1931
Lisse, C. M., Christian, D. J., Dennerl, K., Meech, K. J., Petre, R., Weaver, H. A., & Wolk, S. J. 2001, Science, 292, 1343
Lisse, C. M., et al. 1996, Science, 274, 205
Mumma, M. J., Krasnopolsky, V. A., & Abbott, M. J. 1997, ApJ, 491, L125
Northrop, T. G., Lisse, C. M., Mumma, M. J., & Desch, M. D. 1997, Icarus, 127, 246
Owens, A, et al. 1998, ApJ, 493, L47
Phaneuf, R. A., Alvarez, I., Meyer, F. W., & Crandall, D. H. 1982, Phys. Rev. A, 26, 1892
Suraud, M. G., Hoekstra, R., de Heer, F. J., Bonnet, J. J., & Morgenstern, R. 1991, J. Phys. B, 24, 2543
Unterreiter, E., Schweinzer, J., & Winter, H. 1991, J. Phys. B, 24, 1003
Wang, J., & Kwong, V. H. S. 1997, Rev. Sci. Instrum., 68, 10
Wegmann, R., Schmidt, H. U., Lisse, C. M., Dennerl, K., & Englhauser, J. 1998, Planet. Space Sci., 46, 603
Wickramasinghe, N. C., & Hoyle, F. 1996, Ap&SS, 239, 121